THE INVESTIGATION OF DEPENDENCE OF LOW FREQUENCY MOTION ON UPSTREAM FLOW CONDITIONS IN HYPERSONIC FLOWS

Erinc Erdem*, Konstantinos Kontis*
***School of Mace, University of Manchester, UK**

***Keywords**: Hypersonic flow, viscous interaction, flat plate, experimentation*

Abstract

An experimental study of low frequency viscous interaction is carried out over a flat plate with various Reynolds numbers at a Mach number of 5. Conventional pressure and temperature measurements are carried out with Schlieren photography. The interaction between the boundary layer and oncoming free-stream is found to be of a weak laminar type. The induced pressure levels are compared to analytical/empirical correlations. As Reynolds number is increased the viscous interaction becomes weaker.

Nomenclature

C	Chapman Rubesin linear viscosity law constant
K	Hypersonic similarity parameter
M	Mach number
p	Pressure
Re	Reynolds number
Re/ m	Unit Reynolds number (per unit meter), based on free-stream conditions
T	Temperature

Greek Symbols

δ	Boundary layer thickness
δ^*	Displacement thickness
γ	Ratio of specific heats
μ	Dynamic viscosity
ρ	Density
$\overline{\chi}$	Laminar viscous interaction parameter
$\overline{\chi}_{turb}$	Turbulent viscous interaction parameter

Subscripts

e	Boundary layer edge
x	Distance from the leading edge
w	Wall
∞	Free-stream conditions
0	Stagnation conditions

1 Introduction

Slender vehicles that cruise at very high speeds and re-entry vehicles that glide through the atmosphere have been faced to significant viscous dominated interactions such as strong viscous interactions and/or shockwave-boundary layer interactions during flight. Viscous interaction is defined mainly by the displacement of the outer inviscid flow due to rapid boundary layer growth at the fore front of the vehicle whereas shockwave-boundary layer interaction is created by an impingement of a shock over the laminar/turbulent boundary layer on the surfaces of the vehicle. These interactions complete alter the flowfields over the flying bodies and create regions of high pressure and temperature spots that can cause imminent fatigue of aerostructures and excessive heat transfer rates leading to failure. Even though the density of air is quite low at high altitudes these flow phenomena are still pronounced and significant.

In the high supersonic and hypersonic flow regimes strong viscous interaction occurs if attached boundary layer becomes very large, which is associated with high Mach numbers (M) and relatively low Reynolds numbers (Re). In fact the boundary layer thickness δ is

proportional to $M/\sqrt{\mathrm{Re}_x}$ at these flight regimes. At the leading edge of vehicles sudden growth of boundary layer deflects incoming flow extensively and consequently outer flow sees an effectively thicker body with growing thickness. In return outer flow has to go through a smaller streamtube area and has to change its direction; this occurs with a curved shockwave forming at the leading edge. As a consequence the outer flow at the edge of boundary layer is altered, pressure levels are increased and the changes are fed back to the boundary layer affecting its growth and properties as shown in Fig.1. This mutually interacting flow pattern is called "hypersonic viscous interaction" and it can have important effects on the surface pressure, shear stress and heat transfer distributions of hypersonic vehicles thus modifying their lift, drag and stability characteristics. If this interaction is severe then it is called strong viscous interaction especially occurring in laminar regimes and if it is not considerable, it is called weak viscous interaction [1-5].

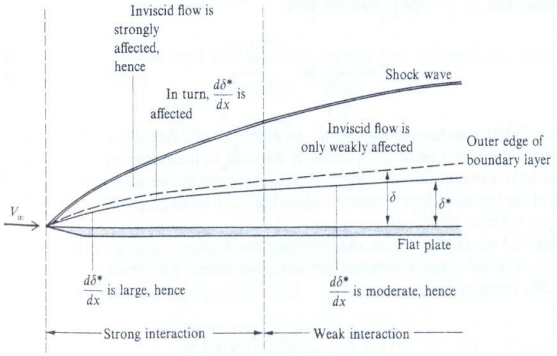

Figure 1 Viscous interaction phenomenon [1]

The pressure distribution over a flat surface in the presence of viscous interaction can be written as a function of hypersonic similarity parameter [1], $K = M_\infty \, d\delta^*/dx$ as shown in Eq.1.

$$\frac{p_e}{p_\infty} = 1 + \frac{\gamma(\gamma+1)}{4}K^2 + \gamma K^2\sqrt{\left(\frac{\gamma+1}{4}\right)^2 + \frac{1}{K^2}} \qquad (1)$$

The pressure at the edge of the boundary is certainly greater than the free-stream pressure due to viscous interaction. Depending on the value of K the strength of the phenomenon varies and some terms drop some prevail. The governing parameter determining how severe this interaction is, is called laminar viscous interaction parameter and given in Eq.2.

$$\overline{\mathrm{X}} = M_\infty^3\sqrt{\frac{C}{\mathrm{Re}_{x\infty}}} \equiv K^2 \qquad (2)$$

where

$$C = \frac{\rho_w \mu_w}{\rho_\infty \mu_\infty}$$

C is named as Chapman Rubesin constant and it assumes linear relationship between viscosity ratio and temperature ratio based on reference temperature concept [1]. If $\overline{\mathrm{X}}$ is smaller, less than three, weak interaction occurs if it is greater than three strong interaction dominates [1, 2]. In fact despite dependence on the incoming flow properties it actually varies along the surface due to local *Re*; at the leading edge it is at its highest and decreases along the plate. Therefore if Re is moderately high and transition location is close to the leading edge turbulent viscous interaction can occur and this is governed by turbulent viscous interaction parameter [2] as depicted in Eq.3.

$$\overline{\mathrm{X}}_{turb} = \left[\frac{M_\infty^9 C}{\mathrm{Re}_{x\infty}}\right]^{0.2} \qquad (3)$$

This study aims at investigation of the relationship between this low frequency laminar/turbulent viscous interaction phenomena and *Re* of the incoming flow. Therefore this program has started with a simple test case, a flat plate in Mach 5 flow to investigate this dependence before advancing to other generic geometries peculiar to high speed flow.

2 Experimental Program

2.1 Experimental Facility

The experiments are conducted in the intermediate blowdown (pressure-vacuum) type highly supersonic/hypersonic tunnel of the

University of Manchester, with air as the test gas at the conditions of $M_\infty = 5$ and various Re_∞ / m values from 4.3 to 14 million. This facility employs a contoured nozzle and free-jet test section accompanied by axially adjustable diffuser in the working section as shown in Fig.2. The variation of *Re* is accomplished by the setting different supply pressures and heater temperatures as upstream stagnation conditions. Maximum stagnation enthalpy of this facility is 0.7mJ/kg and Re_∞ / m range is $3.5\text{-}15*10^6$. The calibration of this facility has been carried out by the author, and flow uniformity (Mach number, *M*) is measured to be less than 1% at different axial stations from nozzle exit. The variation in upstream conditions at the settling chamber during test runs are found to be 0.8% for p_0 and 7% for T_0 respectively. Finally the useful running time of the wind tunnel is about 4 seconds.

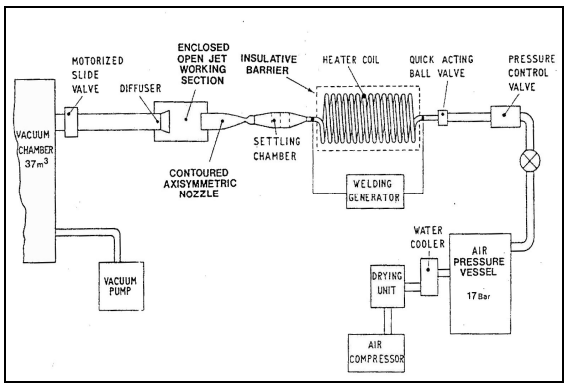

Figure 2 Schematic layout of wind tunnel

The main flow diagnostics used in this study consist of simultaneous pressure and temperature measurements and Schlieren optical visualisation technique.

2.2 Instrumentation and the Model

The stagnation conditions at each test run are measured simultaneously with a pitot probe connected to a 0-15bar ENTRAN X0 pressure transducer and a K-type thermocouple at the settling chamber. Pressure measurements on the flat plate are carried out using Kulite 0-3.5bar XTE-190M pressure transducers with an estimated error of $\pm 2\%$, connected to six pressure tappings on the plate, whose geometry is shown in Fig.3. All the signals are acquired using National Instruments PCI 6251 card at 5 kHz after being conditioned by SCXI-1000 signal conditioning chassis with appropriate modules on it.

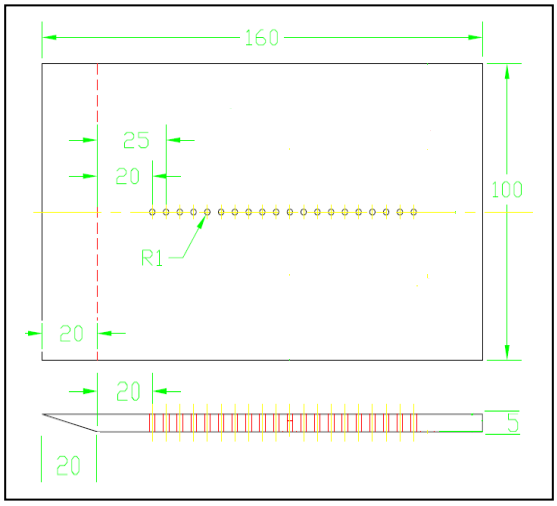

Figure 3 Flat plate configuration (all in mm)

Heat resistant flexible tubing is used to connect pressure tappings at locations 40, 60, 80, 100, 120 and 135mm from the leading edge of the flat plate to pressure transducers placed inside the test section. The calibration of the transducers is carried out inside the test section as it is being vacuumed since the freeestream pressure levels at the test section are quite small at the order of milibars. Additionally the distance between the nozzle exit and the flat plate is kept at 5mm.

2.3 Schlieren Technique

Toepler's z-type Schlieren technique [6] is adapted for flow visualisation that consist of a constant light source of PALFLASH 501 (Pulse photonics) with a focusing lens and a 1.5mm wide slit, two 8" parabolic mirrors with 6ft focal length, a knife edge, a set of HOYA 49mm close-up lenses and a digital Canon SLR, EOS-450D, 12MP. The offset angle between the axis of parabolic mirrors and the axis of the light is set to 3degrees to prevent optical aberrations such as coma and astigmatism [6]. Parallel beam of light is passed through Quartz test section windows of 190mm diameter before focusing on the knife edge plane that is placed perpendicular to flow direction and the focused beam is shone on CMOS sensor of the camera. The camera is set to continuous shooting mode at which it can record 3.5frames/sec at full resolution; the shutter speed is adjusted to

1/4000 sec with an ISO speed of 400 to provide enough detail and appropriate brightness.

3 Results and Discussion

3.1 Upstream and Test Conditions

As previously noted upstream conditions are measured at each test and they are subjected to certain amount of variations during tests therefore it is worthwhile to understand the time history of stagnation conditions as shown in Fig. 4.

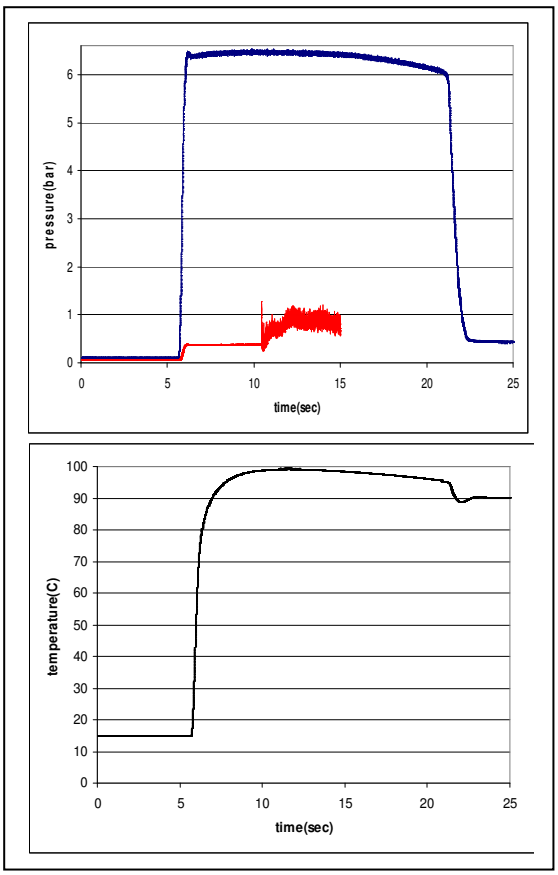

Figure 4 Stagnation pressure and temperature history at 175psi supply pressure and 375K heater temperature with pitot pressure

The pitot probe inserted in test section reveals a plateau shown in the first plot well below the stagnation pressure; it indicates the useful running time of the wind tunnel that is terminated by the normal shock emerging from the diffuser and moving upstream. Within this period of time stagnation pressure shows minor variations however stagnation temperature changes considerably, increasing from vacuum and reaching a value bit lower than the temperature set at the heater.

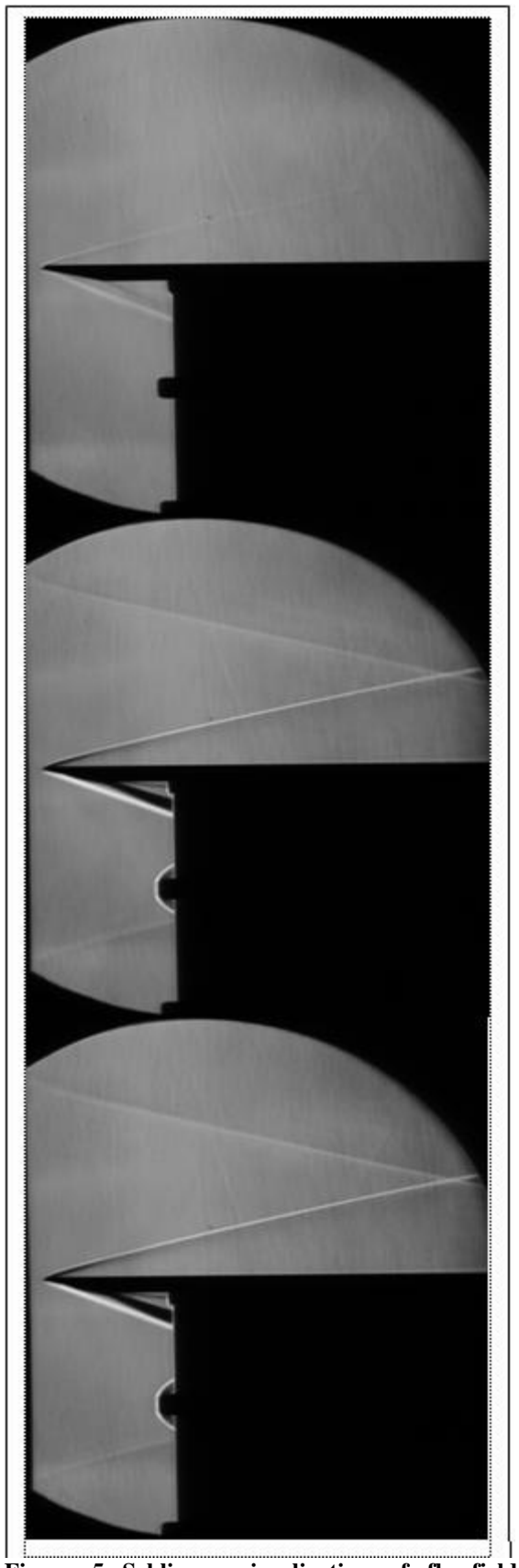

Figure 5 Schlieren visualization of flowfield during test run

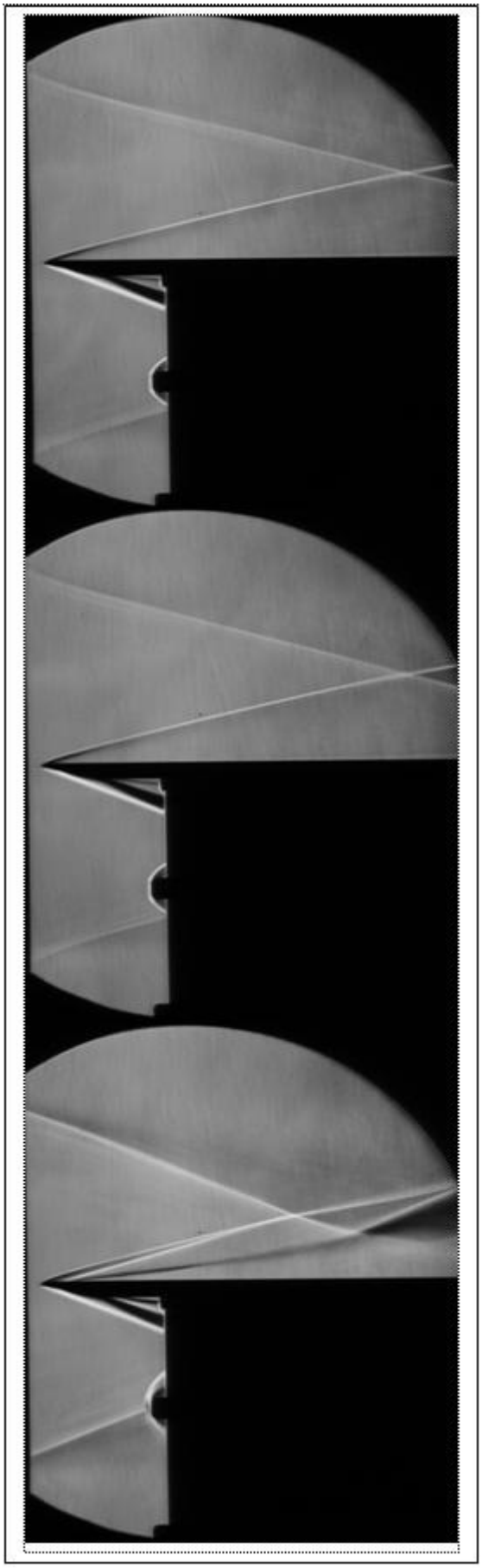

Figure 6 Schlieren visualization continued

Nevertheless the static pressure and temperature in the test section do not undergo significant changes and the flowfield can be assumed to be steady safely as shown from Figures 5 and 6 for the same upstream conditions mentioned above. Only six pictures showing the startup phase, steady phase and ending phase of the useful running time are selected for conciseness.

As the flow starts a curved leading edge shock due to viscous interaction on the top surface starts to appear; an oblique shock and subsequently an expansion fan at the bottom surface occur. There are two oblique shocks emanating from the nozzle exit due to pressure difference between nozzle exit and test section. The top nozzle shock crosses the leading edge shock at downstream of the plate and the boundary layer is vaguely visible and growing over the plate. Flowfield prevails for around 4seconds. Afterwards nozzle shocks start to get closer to the plate from both sides and then due to increasing downstream pressure flow begins to break down and useful running time finishes.

Six test conditions are selected to include different heater temperatures and supply pressures to cover a range of Re_∞/m during the useful running time of the tunnel as shown in Table 1.

Table 1 Test conditions

#	Supply pressure (psi)	p_0 (bar)	Heater temp. (K)	T_0 (K)	Re_∞/m (10^6/m)
1	140	5.46	745	688	4.34
2	150	5.84	625	589	5.76
3	160	6.41	625	600	6.14
4	160	6.34	575	536	7.23
5	175	6.79	475	457	9.95
6	175	6.71	375	366	14.16

Within this range the maximum value of $\overline{\mathrm{X}}$ that can be achieved with this facility is well below three; corresponding to weak laminar/turbulent viscous interaction. Therefore for an insulated plate ($T_w \approx T_0$) and laminar weak interaction ratio of pressures at the boundary layer edge to free-stream pressure is given in Eq.4 and for a cold plate (T_w/T_0 is small) laminar weak interaction formula becomes as in Eq.5 [1, 3]. As observed from

these equations both for air; cold wall reduces the magnitude of viscous interaction since it reduces the boundary layer thickness thus displacement thickness diminishing the cause of viscous interaction [1]. For the turbulent case for air with $\Pr = 1$ the relation is expressed in Eq.6 [2].

$$\frac{p_e}{p_\infty} = 1 + 0.31\overline{X} + 0.05\overline{X}^2 \tag{4}$$

$$\frac{p_e}{p_\infty} = 1 + 0.078\overline{X} \tag{5}$$

$$\frac{p_e}{p_\infty} = 1 + 0.057\left[\frac{1 + 1.3\left(T_w/T_0\right)}{\left[1 + 2.5\left(T_w/T_0\right)\right]^{0.6}}\right]\overline{X}_{turb} \tag{6}$$

For all laminar cases Eq.4, Eq.5 are utilized and compared with experimental results and depending on *Re* turbulent case is utilized. For the calculation of Re_x first tapping position of 40mm from the leading edge is chosen as viscous interaction loses its effect along the plate. For the computation of free-stream conditions isentropic expansion of air through nozzle at the inviscid core of the flow is assumed.

3.2 Test Results

A Schlieren image focused on flow features together with pressure distribution on the flat plate are shown in Fig.7 for test 2. As the flow initiates pressure levels go up and reach a peak then reduce a bit arriving a plateau. As the flow endures pressure levels stay constant with bit of increase compatible with stagnation pressure increase during the tests. Then as the flow breaks down with a shock moving upstream naturally the furthest tapping senses it first then the rest exhibit a jump. In terms of magnitudes first tapping has the highest pressure as expected owing to viscous interaction, however second tapping shows lowest pressure compared to the rest, ideally it should be the second highest, possible reasons might come from boundary layer transition due to both natural causes and roughness implications. Actually starting from second tapping the pressure fluctuations are much more apparent implying transition.

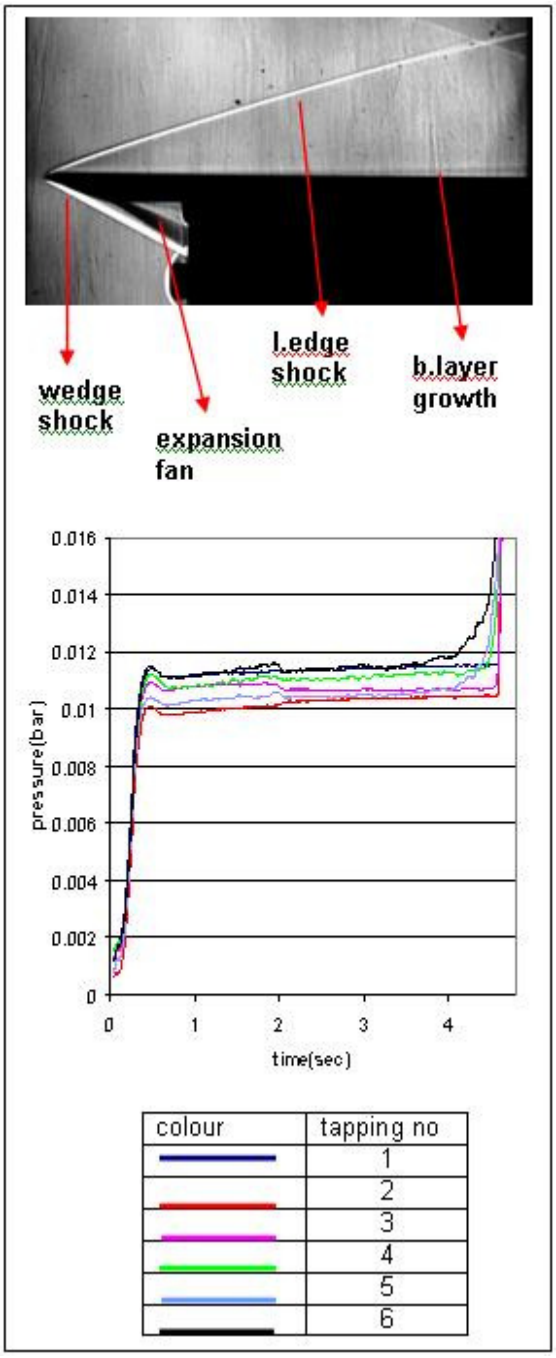

Figure 7 Flow features for test 2 with pressure distribution over the plate

Another reason can be experimental uncertainty such that due to the weak interaction the differences between pressures levels are

quite small and these differences might be buried in uncertainty band. Finally the crossing of leading edge shock and the nozzle shock results a reflected shock that impinges on the plate resulting relatively high pressures at the furthest tapping location.

In order to compare experimental results for different cases with various *Re* with analytical results from viscous interaction relations the plot of non-dimensional wall pressure is drawn against viscous interaction parameter, $\overline{X}$ in Fig.8.

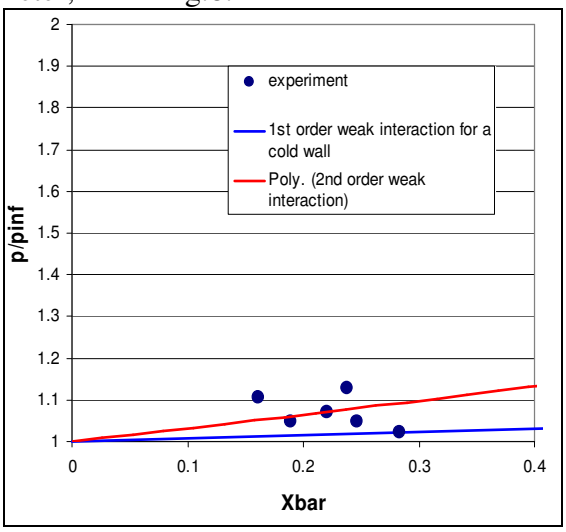

Figure 8 Wall pressure Flow features for test 2

As it can be seen from above figure the weak viscous interaction phenomenon occurring considerably around the leading edge of the flat plate agrees well with the analytical results especially with second-order equation for insulated wall. $\overline{X}$ is changing between test due to changes in *Re* for the same M_∞. Therefore essentially it is showing the dependence of this viscous interaction with incoming *Re*; as it increases the magnitude of interaction decreases, which is shown reasonably by above figure. For test 6 with highest *Re* (around $5.6*10^5$ at tapping location) turbulent weak interaction relation gives a value of 1.076 for pressure ratio instead of 1.051 for laminar case, which is acceptable as well.

Conclusion

An experimental study of viscous interaction is carried out over a flat plate with various Reynolds numbers oat a Mach number of 5. The incoming flow started as laminar and underwent transition for all tests after a certain distance. Due to low Mach number and stagnation temperatures the interaction between suddenly growing boundary layer on the plate and the free-stream is not of a strong type, rather a weak laminar one. The induced pressure levels are compared to analytical/empirical relations at the most front tapping location and the agreement is found to be good. As Reynolds number is increased the effect of interaction is diminished. Schlieren photography provides a valuable insight of the flow field and viscous interaction phenomenon.

References

[1] Anderson J. D. *Hypersonic and High Temperature Gas Dynamics.* 2nd edition, AIAA, 2006.

[2] Hirschel E. H. Basics of Aerothermodynamics. 1st edition, Springer & AIAA, 2005.

[3] Cox R. N., Crabtree L.F. *Elements of Hypersonic Aerodynamics*. 1st edition, English Universities Press, 1965.

[4] Bertin J. J. *Hypersonic Aerodynamics*. 2nd edition, AIAA, 1994.

[5] White F. M. *Viscous Fluid Flow*. 3rd edition, McGraw Hill, 2006.

[6] Settles G. *Schlieren and shadowgraph techniques*. 1st edition, Springer, 2001.

Copyright Statement